JACS
JOURNAL OF THE AMERICAN CHEMICAL SOCIETY
Article
pubs.acs.org/JACS

Free H_2 Rotation vs Jahn–Teller Constraints in the Nonclassical Trigonal (TPB)Co–H_2 Complex

William A. Gunderson,[†] Daniel L. M. Suess,[‡] Henry Fong,[‡] Xiaoping Wang,[§] Christina M. Hoffmann,[§] George E. Cutsail III,[†] Jonas C. Peters,*[,‡] and Brian M. Hoffman*[,†]

[†]Department of Chemistry, Northwestern University, Evanston, Illinois 60208-3113, United States
[‡]Division of Chemistry and Chemical Engineering, California Institute of Technology, Pasadena, California 91125, United States
[§]Chemical and Engineering Materials Division, Neutron Sciences Directorate, Oak Ridge National Laboratory, Oak Ridge, Tennessee 37831-6475, United States

Supporting Information

ABSTRACT: Proton exchange within the M–H_2 moiety of (TPB)Co(H_2) (Co–H_2; TPB = B(*o*-$C_6H_4P^iPr_2)_3$) by 2-fold rotation about the M–H_2 axis is probed through EPR/ENDOR studies and a neutron diffraction crystal structure. This complex is compared with previously studied (SiP^{iPr}_3)Fe(H_2) (Fe–H_2) (SiP^{iPr}_3 = [Si(*o*-$C_6H_4P^iPr_2)_3$]). The *g*-values for Co–H_2 and Fe–H_2 show that both have the Jahn–Teller (JT)-active ^2E ground state (idealized C_3 symmetry) with doubly degenerate frontier orbitals, $(e)^3 = [|m_L \pm 2>]^3 = [x^2 - y^2, xy]^3$, but with stronger linear vibronic coupling for Co–H_2. The observation of ^{1}H ENDOR signals from the Co–HD complex, ^{2}H signals from the Co–D_2/HD complexes, but *no* ^{1}H signals from the Co–H_2 complex establishes that H_2 undergoes proton exchange at 2 K through rotation around the Co–H_2 axis, which introduces a quantum-statistical (Pauli-principle) requirement that the overall nuclear wave function be antisymmetric to exchange of identical protons (I = 1/2; Fermions), symmetric for identical deuterons (I = 1; Bosons). Analysis of the 1-D rotor problem indicates that Co–H_2 exhibits rotor-like behavior in solution because the underlying C_3 molecular symmetry combined with H_2 exchange creates a dominant 6-fold barrier to H_2 rotation. Fe–H_2 instead shows H_2 localization at 2 K because a dominant 2-fold barrier is introduced by strong Fe(3d)→ $H_2(\sigma^*)$ π-backbonding that becomes dependent on the H_2 orientation through quadratic JT distortion. ENDOR sensitively probes bonding along the L_2–M–E axis (E = Si for Fe–H_2; E = B for Co–H_2). Notably, the isotropic ^{1}H/^{2}H hyperfine coupling to the diatomic of Co–H_2 is nearly 4-fold smaller than for Fe–H_2.

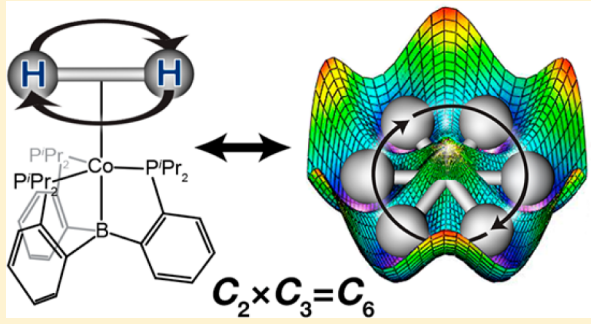

INTRODUCTION

The M–H_2 moiety has been described as "among the most dynamic, complex, and enigmatic chemical topologies",[1] with a particularly interesting aspect being the exchange of the identical hydrons of H_2/D_2 through 2-fold rotation about the M–H_2 axis.[1−4] This exchange correlates the nuclear spatial and spin states, as with *o*- and *p*-H_2,[5] because of the Pauli-principle (quantum-statistical) requirement that the overall nuclear wave function must be antisymmetric to exchange of identical protons (I = 1/2; Fermions), but symmetric to exchange of identical deuterons (I = 1; Bosons). These correlations control the nature of the NMR spectra of diamagnetic H_2/D_2 complexes,[4,6] and the hyperfine interactions observable in the EPR and ENDOR spectra for nonclassical paramagnetic M–H_2 complexes, the latter being corollaries to McConnell's recognition of the role of these quantum-statistical considerations in paramagnetic resonance spectroscopies.[7]

Studies of M–H_2 adducts, beginning with the paradigmatic pseudo-octahedral, d^6 tungsten complex of Kubas (Figure 1)[8,9] have shown that the rotational dynamics are exceptionally sensitive to the ancillary ligands,[1,10−12] most notably the *cis* ligands,[11,13,14] and to the structure and bonding of the complex,[9,15,16] as well as the nonbonded environment of the M–H_2 moiety.[15] In a variety of such complexes it has been found that the H_2 ligand rotates on an adiabatic potential

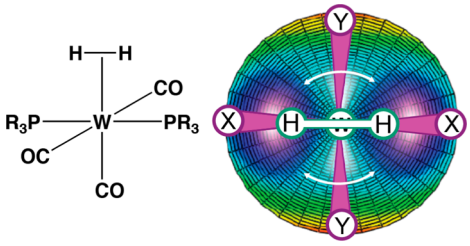

Figure 1. Schematic representation of the APES for rotation of the H_2 of a pseudo-octahedral M–H_2 complex, such as the Kubas tungsten complex illustrated at left.

Received: August 7, 2014
Published: September 22, 2014

   dx.doi.org/10.1021/ja508117h | *J. Am. Chem. Soc.* 2014, 136, 14998–15009

energy surface (APES) dominated by a 2-fold barrier to rotation, as illustrated in Figure 1.[17] The 2-fold barrier strongly quenches rotor-like behavior, normally lowering the energy spacing ("tunnel splitting") between the ground rotational state (symmetric to Hydron interchange) and the first-excited state (antisymmetric to exchange) from the value $\Delta = 40-50$ cm^{-1} for free rotation of an H_2 ligand stretched by covalency with M,[18,3] to the order of several cm^{-1} or less, as determined by inelastic neutron scattering (INS)[3,15] or NMR.[4,6] As a consequence, the H_2 ligand is effectively localized within the rotational energy minima generated by the 2-fold barrier, and the hydrons exchange by 180° tunneling and/or hopping between minima.

The mononuclear M−H_2 adducts, (SiP^{iPr}_3)Fe(H_2) (Fe−H_2) and (TPB)Co(H_2) (Co−H_2) (where SiP^{iPr}_3 = [Si(*o*-$C_6H_4P^iPr_2)_3$]$^-$, TPB = B(*o*-$C_6H_4P^iPr_2)_3$), Figure 2, are the only known examples of well-characterized, "nonclassical", paramagnetic ($S = 1/2$) metal complexes with a coordinated dihydrogen ligand.[19,20] These M−H_2 complexes are unique in that the H_2 ligand is bound at a metal site with idealized C_3 symmetry (Figure 2, lower, left), in contrast with the C_2 or C_4 symmetry of prototypical M−H_2 complexes. The idealized C_3 symmetry of Fe−H_2 and Co−H_2 results in an electronic structure with a ^2E ground state that is susceptible to a symmetry-lowering "pseudo-Jahn−Teller" (PJT) distortion,[21−23] and this has a profound impact on the dynamics of H_2 rotation at cryogenic temperatures. Our recent study[20] of Fe−H_2 at 2 K reported ^{1}H ENDOR signals from the ground rotational state of the coordinated H_2 ligand, and thus the absence of Pauli-principle constraints, thereby ruling out the possibility that Fe−H_2 exhibits free rotor-like behavior. Instead, the H_2 ligand is strongly localized and tunnels among energetic minima, as do the prototypical H_2 complexes,[17,24,25] but in an unusual fashion that rotationally averages the hyperfine interaction without Hydron exchange.

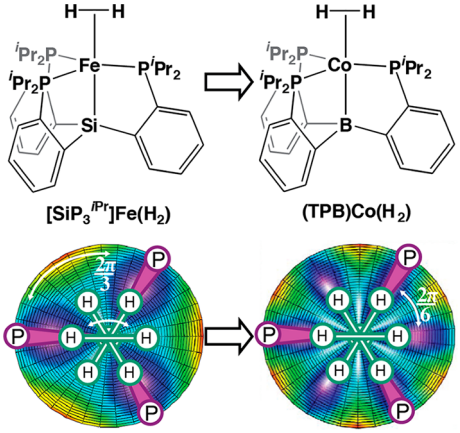

Figure 2. (Upper) Trigonal M−H_2, M = Fe, Co, complexes. (Lower) Schematic representation of the apparent spatial C_3 APES for rotation of the H_2 of a trigonal M−H_2 complex (left) and of the actual C_6 surface (right) generated by incorporation of exchange of the two H/D through a 2-fold rotation.

We now report EPR/ENDOR studies of Co−H_2 that show that the dynamics of H_2 rotation in Co−H_2 are sharply different from those in Fe−H_2: the H_2 ligand of Co−H_2 at 2 K acts as a free rotor, with Pauli-principle correlation between spatial and nuclear-spin states. Theoretical analysis of the 1-D rotor problem, along with a neutron diffraction study of Co−H_2, indicates that both complexes undergo a static quadratic JT distortion, but that this distortion is smaller for Co−H_2. As a result, Co−H_2 exhibits rotor-like behavior in solution as the manifestation of a dominant 6-fold rotational barrier to H_2 rotation introduced by the underlying C_3 molecular symmetry in conjunction with H_2 exchange. In contrast, H_2 localization in solution is observed for Fe−H_2 as the manifestation of a dominant 2-fold barrier introduced by Fe(3d) → $H_2(\sigma^*)$ π-backbonding that is enabled by its JT distortion.

MATERIALS AND METHODS

Sample Preparation. All manipulations were carried out using a standard glovebox or Schlenk techniques. Co−H_2, Co−D_2, and Co−HD were prepared according to literature procedures.[19] THF, 2-Me-THF, toluene, HMDSO, and methylcyclohexane were rigorously dried by stirring over Na metal for several days followed by filtration through a pad of activated alumina. HD gas was generated by the slow addition of D_2O into $LiAlH_4$. Q-band ENDOR tubes were charged with the Co−H_2 or Co−D_2 solutions under an atmosphere of the respective dihydrogen isotopologue.

As the foundation of this report is the *absence* of the ^{1}H ENDOR signal from Co−$^1H_2$, despite the *presence* of the ^{2}H ENDOR signal from Co−$^2H_2$, three separate sets of Co−$^1H_2$ samples in both toluene and 9:1 THF:2Me-THF were prepared for ENDOR analysis: all gave equivalent results. All spectra presented were obtained with a 9:1 THF:2-MeTHF solvent mixture.

Co−H_2 crystals of suitable size for single crystal-neutron diffraction were grown under 1 atm of H_2 in a J-Young NMR tube according to the following procedure. A suspension of Co−H_2 in 2:1 HMDSO:methylcyclohexane at room temperature (RT) was dissolved by heating to 90 °C in an oil bath. The sample was then allowed to cool to RT in the oil bath, which was left undisturbed for 3 days, yielding large yellow crystals of Co−H_2.

ENDOR Spectroscopy. 35 GHz (Q-band) field-modulated, continuous-wave (cw) ENDOR spectra were recorded at 2 K with a helium immersion dewar by digitization of the output signal from a modified Varian E-110 spectrometer. Signal intensity was improved through noise broadening of the swept RF.[26]

Pulsed Q-band ENDOR spectra were collected at 2 K on a home-built instrument, as described previously.[20] Experiments were performed using the Davies ($\pi-\tau-\pi/2-T-\pi-\tau-$echo) "3-pulse" microwave sequence where the RF is applied during time period T. Data acquisition was performed with the SpecMan software package (http://www.specman4epr.com).[27] The ENDOR spectrum from an $I = 1/2$ nucleus (^{1}H) shows a doublet at frequencies

$$\nu_{\pm} = |\nu_n \pm A/2| \quad (1)$$

where ν_n is the nuclear Larmor frequency and A is the hyperfine coupling. When $I \geq 1$ (^{2}H,^{11}B), a nuclear quadrupole interaction (P) in principle can introduce further splitting of the $\nu_{\pm}$ manifolds, but these splittings were not resolved here. Complete hyperfine tensors are obtained by analysis of the 2-D field-frequency pattern consisting of ENDOR spectra collected at numerous fields across the EPR signal of the paramagnetic center (e.g. ref 20).

Neutron Diffraction. Single crystal neutron diffraction data were measured on the TOPAZ instrument at the Spallation Neutron Source at Oak Ridge National Laboratory, in the wavelength-resolved time-of-flight Laue diffraction mode using wavelengths in the range 0.4−3.5 Å.[28] A rod-shaped crystal of Co−H_2 with the dimensions of 0.42 × 0.60 × 1.20 mm^3 was mounted onto the tip of a polyimide capillary with fluorinated grease in a nitrogen glovebox, and transferred onto the TOPAZ goniometer for data collection at 100 K. To ensure good coverage and redundancy, data were collected using 26 crystal orientations optimized with CrystalPlan software.[29] Each orientation was measured for approximately 5.9 h.

The integrated raw Bragg intensities were obtained using the 3-D reciprocal Q-space integration method in Mantid,[30] where $Q = 2\pi/d = 4\pi(\sin\theta)/\lambda$. The peaks from Co−$H_2$ were found to be triplets in Q-

dx.doi.org/10.1021/ja508117h | J. Am. Chem. Soc. 2014, 136, 14998−15009

space within less than 0.15 $Å^{-1}$ radii. Bragg peaks from the major component were used for determination of orientation matrix for the Co−H_2 crystal. Peak integration was performed accordingly using a radius of 0.15 $Å^{-1}$ to include contributions from all three components. Data reduction for each sample, including neutron TOF spectrum, detector efficiency, and absorption corrections, was carried out with the ANVRED2 program.[31] The reduced data were saved in SHELX HKLF2 format in which the wavelength is recorded separately for each individual reflection, and were not merged as a consequence of this saved format. The initial structural model used the unit cell parameters and non-hydrogen atom positions from the single-crystal XRD experiment measured at 100 K. The hydrogen atoms were found from nuclear difference Fourier map of the neutron data, and refined anisotropically using SHELXL-97[32] in WinGX.[33]

The dihydrogen ligand was found to be disordered in two positions with the site occupancy factors refined to 68.2 and 25.2%, respectively, for the major and minor components. The remaining 6.6% nuclear density was modeled as a bromide ligand at 2.383(13) Å away from the Co center and is attributed to residual Co−Br starting material. The neutron structure was validated with Platon and the IUCr online checkcif program. The following is a list of programs used: orientation matrix from live neutron event data, ISAW Event Viewer; data collection strategy, CrystalPlan; Data collection, SNS PyDas; data reductions, Mantid; absorption correction, ANVRED2; structural refinement, SHELXL-97;[32] promolecule isosurface plots, CrystalExplore.[34]

RESULTS AND ANALYSIS

PJT Effects and the EPR Spectroscopy of Co−H_2 and Fe−H_2. The reported[19] g-tensor for low-spin Co−H_2, **g** = [2.457, 2.123, 2.029], is roughly axial, with $g_{\|} = g_1 > (g_2, g_3) \sim g_{\perp} \sim g_e$, as is the case[20] for low-spin Fe−H_2, **g** = [2.275, 2.064, 2.015]).[35,36] The similarity of the EPR spectra for Co−H_2 and Fe−H_2 implies that they have the same ^2E ground states (idealized C_3 symmetry) whose frontier orbitals are the triply occupied, orbitally degenerate doublet configuration $(2e)^3 = [|m_L \pm 2\rangle]^3 = [x^2 - y^2, xy]^3$, as depicted in Figure 3. This

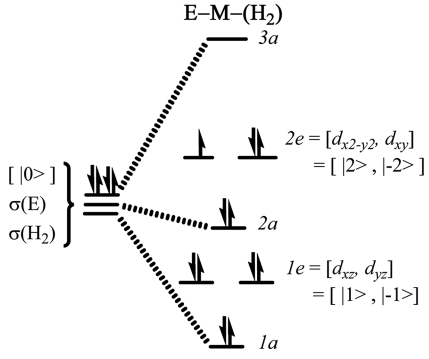

Figure 3. Orbital scheme for E−M−H_2 complexes, E = B or Si, M = Co or Fe, in idealized trigonal symmetry: $|0\rangle = d_{z2}$ of M; σ(E) = sp hybrid orbital on E; $\sigma(H_2)$ = bonding orbital of H_2. The relative order of the fully occupied orbitals may vary depending on the identity of M and E.

similarity arises because the two complexes have the same total number of valence electrons, {Co−B}[9] and {Fe−Si}[9], even though the two complexes can be viewed formally as having either d^9 (Co(0) and Fe(1−)) or d^7 (Co(2+) and Fe(1+)) electron counts. The resulting ^2E state is susceptible to the "pseudo-Jahn−Teller" (PJT) effect wherein spin−orbit coupling competes with interactions that lower the idealized C_3 molecular symmetry.[21] Foremost among the interactions are (i) vibronic coupling to a symmetry-lowering distortion along an "interaction" e vibrational coordinate; (ii) π-backbonding from the lower-lying, fully occupied orbital pair, $(d\pi)^4 = (1e)^4 = [|m_L \pm 1\rangle]^4 = [xz, yz]^4$, to the unoccupied antibonding $H_2(\sigma^*)$ orbital;[1−3,16] (iii) noncovalent interactions with the molecular environment and/or crystal packing effects in a crystal.

In the PJT effect, linear vibronic coupling replaces the ^2E electronic degeneracy with a vibronic degeneracy in which the complex is dynamically distorted (e.g., equilateral ↔ isosceles triangle of P atoms), with the direction of the distortion "pseudorotating" around the symmetry axis.[22,23] However, as is well-known,[22,23] and recently seen elsewhere,[37] incorporation of quadratic terms in the vibronic interaction "warp" the potential energy surface for the PJT distortion, generating three equivalent distorted conformations that might correspond, for example, to stabilization of the three equivalent isosceles triangles formed by appropriate displacements of the P atoms, with a barrier to conversion between the three distorted conformations.[22,23]

The g-tensor of the Co−H_2 and Fe−H_2 complexes can be described through a formal analysis of the linear PJT effect[21] that is formulated in terms of a dimensionless parameter, $r = 2V/\lambda$ (eq 2). The numerator is a sum of two types of terms, $V = V_{vib} + V_l$. The first term is the linear vibronic coupling energy, $V_{vib} = F\rho_0$, F being the coupling constant to the interaction coordinate and ρ_0 being the equilibrium displacement in that coordinate; $\rho_0 \sim F/K$, where K is the force constant of this coordinate. The second term in the numerator, V_l, includes noncovalent contributions. The denominator, λ, is the spin−orbit coupling (SOC) parameter, which traditionally is taken to be the ionic SOC constant, λ_{SOC}, multiplied by a "covalency parameter", k, defined such that $(1 - k)$ represents the fraction of d-electron density delocalized onto the ligands. The energies and wave functions of the distorted state are fixed by r, and are conveniently parametrized in terms of a fictitious angle, 2θ.

$$\tan 2\theta \equiv r = \frac{2V}{\lambda} \qquad \lambda = k\lambda_{SOC} \tag{2}$$

The g values for the ground Kramers doublet of the distorted $[e_2]^3$ state can be written as a function of this angle:

$$g_{\|} = 2(1 + k\cos(2\theta))$$
$$g_{\perp} = 2\sin(2\theta) \tag{3}$$

In principle, the angle, θ, and thus the ratio, r, can be determined from $g_{\perp}$, and the parameter k then be determined from $g_{\|}$. In the case of the two M−H_2 complexes of present interest, however, $g_{\perp} = (g_2 + g_3)/2 > 2$, contrary to eq 3. This implies that the small deviations of g_2 and g_3 from g = 2 are modified by terms that arise from SOC to other d orbitals, and are not solely determined by the PJT. Assuming a value of $k \sim 0.8$ for both M−H_2 complexes, a plausible value for d-electron delocalization, and using tabulated values,[38] λ_{SOC}(Fe) = 335, λ_{SOC}(Co) = 390 cm^{-1},[39] the nearly 2-fold difference between $\delta g_{\|} = (g_{\|} - 2)$ for the two M−H_2 complexes ($\delta g_{\|} \sim 0.28$, $r \sim 11$ for Fe; $\delta g_{\|} \sim 0.46$, $r \sim 7$ for Co) corresponds to a 2-fold greater value for the vibronic coupling. As discussed below, this difference contributes majorly to differences in the H_2 rotational dynamics of the Co and Fe complexes.

^{1,2}H ENDOR of Co−H_2/D_2/HD. Figure 4 presents 35 GHz pulsed ^{1,2}H ENDOR spectra collected for Co−H_2/D_2 at 2 K. The ^{1}H spectra for both isotopologues show a narrow,

dx.doi.org/10.1021/ja508117h | J. Am. Chem. Soc. 2014, 136, 14998−15009

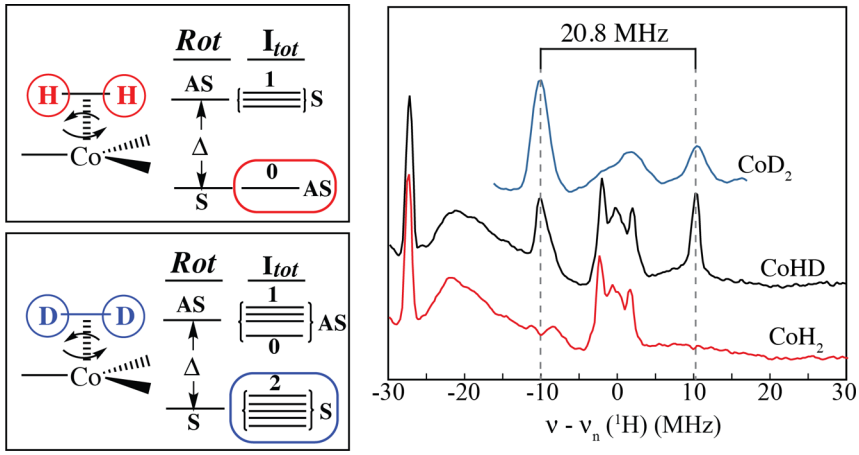

Figure 4. Left: Spatial rotational (Rot) energy levels and corresponding total nuclear spin (I_{tot}) states for Co−H_2 and Co−D_2. The ground rotational state for each species is symmetric (S) to Hydron exchange; the lowest-lying state antisymmetric (AS) to exchange and corresponding spin state(s) as indicated. Right: Q-band Pulsed Davies ENDOR spectra of Co−H_2 (red lines), Co−D_2 (blue lines), and Co−HD (black line) at g_3 = 2.03. Markers indicate A(^{2}H) = 3.2 MHz, and the corresponding coupling for ^{1}H (20.8 MHz). The broad feature from ∼ −25 to ∼ −5 MHz in the ^{1}H spectra of Co−HD and Co−H_2, and seen for Co−D_2 as well (not shown), is the ^{31}P ENDOR response. The frequency axis for the Co−D_2 spectrum has been scaled to match that of the Co−HD and Co−H_2 spectra. The ^{2}H ENDOR spectrum of Co−HD (not shown) shows the same ^{2}H features as that of Co−D_2. Conditions: Davies ENDOR, MW frequency = 34.817 GHz, B = 12255 G, τ = 700 ns, T = 2 K, t_{90} = 80 ns, t_{180} = 160 ns, T_{rf} = 30 μs.

unresolved feature centered at ν_H arising from weakly coupled protons of the ancillary ligand. Neither isotopologue shows a signal from strongly coupled ^{1}H nuclei. Co−D_2, however, shows a hyperfine-split doublet with A(^{2}H) = 3.2 MHz for the bound D_2. Adjusting for the difference in gyromagnetic ratios ($\gamma(^1H)/\gamma(^2H)$ = 6.51), this would correspond to a strong ^{1}H hyperfine coupling for bound $^1H_2$, A(^{1}H) = 20.8 MHz, which would be readily detected in the ^{1}H ENDOR measurement. Indeed, Fe−H_2/D_2 shows just such corresponding ^{1}H and ^{2}H signals.[20] However, Co−HD shows the hyperfine-split ^{1}H signal that is absent in Co−H_2, as well as the expected ^{2}H doublet (Figure 4). As required, the ^{1}H hyperfine coupling for the HD proton, A(^{1}H) = 20.8 MHz, corresponds to the ^{1}H coupling calculated through scaling the ^{2}H coupling of Co−D_2 (or Co−HD). To confirm that the absence of such a ^{1}H signal for Co−H_2 is not attributable merely to a low signal-to-noise ratio, we performed experiments on three separate sets of samples of Co−H_2 and saw identical results: no $^1H_2$ signal even though the ^{1}H signals from the weakly coupled ^{1}H nuclei of the ancillary ligand (as also observed for Fe−H_2), and the signal from the proximal ^{11}B were observed with comparable intensities to those in the spectra from Co−D_2 and Co−HD (see below).

The observation of strongly coupled ^{1}H signals from the Co−HD complex, ^{2}H ENDOR signals from the Co−D_2/HD complexes, but *no* ^{1}H signals from the Co−H_2 complex requires that the two H atoms of H_2 are undergoing exchange through rotation around the Co−H_2 axis, which introduces constraints to the H_2 wave function introduced by the quantum statistics of Hydron exchange.[40] For identical dihydrogen isotopologues, L_2, the Pauli exclusion principle requires that the total nuclear wave function, which is a product of spatial and spin functions, must have a definite parity with respect to exchange of the hydrons:[5,7] antisymmetric for the Fermions (I = 1/2) of $^1H_2$; symmetric for the bosons (I = 1) of D_2. The spatial nuclear ground state of an L_2 rotor is symmetric (S) to exchange, so the spin function for the two ^{1}H Fermions must then be antisymmetric, a *para*-state with antiparallel nuclear spins and total nuclear spin I_{tot} = 0. Such a state *cannot* show a ^{1}H ENDOR signal, in agreement with the results for Co−H_2 at 2 K (Figure 4). Conversely, for a symmetric spatial nuclear ground state, the nuclear spin state of Co−D_2 must also be symmetric. The I = 1 deuteron spins couple to form states of total nuclear spin with I_{tot} = 0, 1, or 2; of these, only the I_{tot} = 2 state is symmetric to interchange of the deuterons, and thus only it can be associated with the spatially symmetric ground state. This spin state does have ENDOR transitions, as observed for Co−D_2 (Figure 4). As the hydrons of the HD diatomic are not equivalent, there is no exclusion-principle restriction to the ENDOR responses, which are thus allowed for both the ^{1}H and ^{2}H nuclei regardless of the spatial nuclear state.

An excited spatial state of Co−H_2 that is antisymmetric (AS) to nuclear exchange would exhibit ^{1}H ENDOR signals, because it must correspondingly have a symmetric nuclear spin state, which means the state with total nuclear spin, I_{tot} = 1. The absence of any ^{1}H signals from Co−H_2 implies that the lowest-lying AS spatial state is negligibly populated at 2 K; the absence of any detectable signal indicates that the excitation energy to such a state can be no less than $\Delta > 7$ cm^{-1}. This *lower bound* to Δ is notably greater than typical values,[1] $\Delta \sim 1$ cm^{-1}, and indeed greater than all but a few splittings measured for transition-metal H_2 adducts.[11,13,15]

^{1,2}H Hyperfine Tensor of Co−H_2/D_2. Figure 5 presents a 2-D field-frequency pattern of ^{2}H ENDOR spectra for Co−D_2 taken at multiple fields across the EPR envelope. The ^{2}H quadrupolar splitting is expected to be less than 100 kHz,[4] and the widths of the individual ν_+/ν_- branches (∼400 kHz) in the ENDOR spectrum are too great to permit their resolution. The deuteron signals for Co−D_2 (and Co−HD) are narrower than those of the proton signals for Co−HD, indicating that the widths scale with the actual value of the hyperfine coupling, and thus are dominated by a slight distribution in the coupling.

The 2-D pattern is simulated by hyperfine coupling to a single type of ^{2}H nucleus with a coupling tensor **A**(^{2}H) = +[3.65, −3.6, −3.25] MHz, which corresponds to **A**(^{1}H) =

dx.doi.org/10.1021/ja508117h | J. Am. Chem. Soc. 2014, 136, 14998−15009

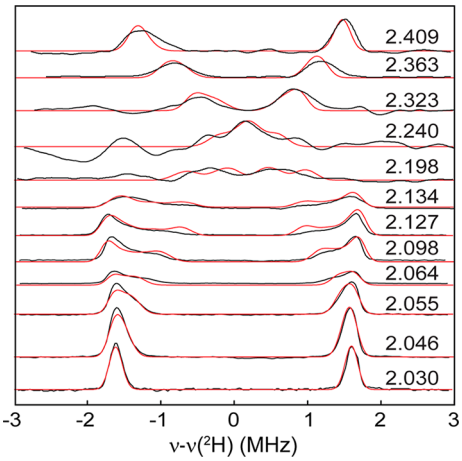

Figure 5. 2-D ^{2}H CW ENDOR pattern for Co−D_2 (black lines) and simulations (red lines). Magnetic fields and *g*-values are indicated. For clarity the ^{1}H ENDOR pattern has been subtracted to remove the ^{11}B signal. Simulation parameters: **g** = [2.46, 2.12, 2.03]; **A** = [3.65, −3.6, −3.25] MHz; (α, β, γ) = (0, 0, 0); EPR/ENDOR line width = 150/0.2 MHz. Conditions: microwave frequency = 35.295 GHz, modulation amplitude = 0.5 G, RF sweep rate = 2 MHz/sec, time constant = 32 ms.

+[23.8, −23.4, −21.2] MHz upon scaling by the ratio of the nuclear *g*-factors. This corresponds to an isotropic coupling $a_{iso}(^1H)$ = −6.9 MHz, and an anisotropic coupling $\mathbf{T}(^1H)$ = +[30.7, −16.5, −14.2] MHz. The sign of a_{iso} is determined by the sign of **T**, which originates in the through-space, electron−nuclear Co−H dipolar hyperfine coupling, and must have a positive sign.[41] The Fe−H_2 complex exhibits a similar dipolar term ($\mathbf{T}(^1H)$ = +[27.7, −15.2, −12.4] MHz) but an isotropic coupling with a much larger magnitude ($a_{iso}(^1H)$ = −25.4 MHz).[11]

For discussion of H_2/D_2 dynamics, the critical parameter in the ENDOR simulations is the value of the angle, β, made by the g_1 and $T_1(^2H)$ principal axes. For a static, symmetric M−H_2 geometry, the measured β would correspond to the structural angle, β_s, between g_1 and the M−H vector(s), Chart 1. Taking

Chart 1

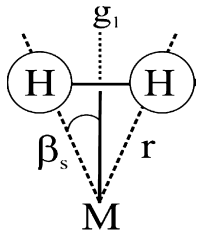

the neutron-diffraction structure of the Co−H_2 fragment (average values, d_{H-H} = 0.83 Å; d_{Co-H} =1.67 Å; see below), the H atoms would exhibit a geometrically determined angle, β_s ~ 15°. However, the 2-D pattern of orientation-selective ^{2}H ENDOR spectra for Co−D_2, Figure 5, is well simulated with β = 0, which indicates that the Co−D_2 is rotor-like, with a distributed ground state in which the ^{2}H electron−nuclear dipolar interaction is averaged to zero.

The measured value of the unique component of the averaged dipolar interaction, $T_1 \equiv 2T'$, is related to the geometry of the Co−D_2 moiety (Chart 1) through the relationship, $2T' = [(3\cos^2\beta_s - 1)]T$, where $T = g_e g_n \beta_e \beta_n / r^3$. The dipolar parameter for Co−H_2, $2T'$ = 30.7 MHz, corresponds to a Co−H distance of r ~ 1.73 Å, slightly greater than given by the neutron structure, but in satisfactory agreement, given the simplifications involved in the use of the point-dipole model.[42−44] The previous measurements for Fe−H_2 yielded an apparent angle between g_1 and the Fe−H vector of β = 6°, which was interpreted as indicative of partial rotational averaging of the dipolar interaction.[20] In this case, $2T' = [(3\cos^2\beta_s - 1)/(3\cos^2\beta - 1)]2T$, which yields an estimated Fe−H distance, r ~ 1.71 Å, within error the same as for Co−H_2.

^{11}B ENDOR of Co−H_2. Figure 6 presents the 2-D field-frequency 35 GHz CW ENDOR pattern of ^{11}B signals collected

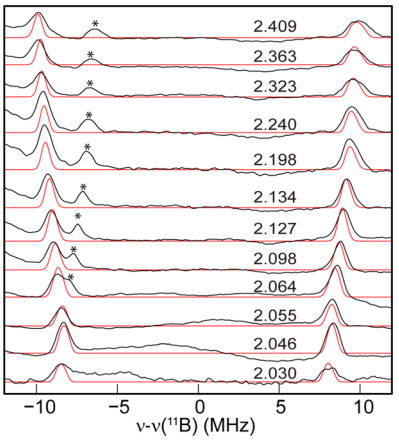

Figure 6. Q-band CW ^{11}B ENDOR of Co−H_2 (black lines) and simulations (red lines) at *g*-values as indicated. Simulation parameters: **g** = [2.46, 2.12, 2.03]; **A** = −[20, 17, 17] MHz; (α, β, γ) = (0, 0, 0); EPR/ENDOR line width = 200/0.2 MHz. Conditions: mw frequency: 35.295 GHz modulation amplitude = 1.0 G, RF sweep rate, 2 MHz/sec; time constant = 32 ms, T = 2 K.

across the EPR envelope of the Co−H_2 complex. Each spectrum shows an ^{11}B doublet centered at υ_B and split by the orientation-dependent hyperfine coupling, without additional resolved quadrupole splitting. The pattern is well-simulated with a hyperfine tensor, **A** = −[20, 17, 17] MHz, coaxial to **g**, corresponding to an isotropic coupling, a_{iso} = −18 MHz. We were unable to determine the sign of **A** using PESTRE measurements;[45] we assign **A** < 0 because the isotropic coupling is essentially the same as that for the isoelectronic complex, [K(18-crown-6)$_2$][(TPB)Fe(N_2)], for which the signs were determined, a_{iso} = −19.5 MHz.[46] The isotropic coupling corresponds to <0.01 electron spin density,[39] and the small dipolar coupling implies that spin density in 2p orbitals of ^{11}B is comparably small.

The absence of resolved quadrupole splittings from the I = 3/2 ^{11}B nucleus at any value of the observing magnetic field indicates that this splitting is much less than the ~1 MHz line widths. A quadrupole coupling so close to zero implies a nearly spherical *electron density* at boron, and that the electron density in the 2p component of the boron sp^n orbital involved in the H_2−M−B four-electron, three-center σ bonding is similar to the 2p density on B in the B−C bonds of the ancillary ligand.[47]

H_2 Rotation/Exchange in the PJT-Active Trigonal M−H_2 Complexes. In this section we first describe the quantum mechanical treatment of H_2 rotation in an *n*-fold barrier to rotation, and show that it predicts remarkably different behavior for 2-fold (Figure 1) and 3-fold symmetric complexes (Figure

dx.doi.org/10.1021/ja508117h | J. Am. Chem. Soc. 2014, 136, 14998−15009

2). With this foundation we then explain the remarkable rotor-like behavior of Co−H_2 and its sharp difference from the behavior of Fe−H_2.

Quantum-Mechanical Treatment of the 1-D Rotor Subject to an n-Fold Rotational Barrier. Spatial rotations are treated with the model of a 1-D quantum mechanical rotor in which the orientation is described with a single degree of rotational freedom (rotational angle, ϕ). Hindrance to free rotation by the molecular environment is modeled by an APES dominated by the appropriate harmonic barrier potential, $V_n(\varphi)$, of depth V_n. The corresponding Hamiltonian is

$$\hat{H} = \frac{h^2}{2I}\hat{L}_z^{\,2} + V_n(\phi) \quad V_n(\phi) = \frac{V_n}{2}(1 - \cos(n\phi)) \tag{4}$$

where L_z is the dimensionless angular momentum operator for rotation about the symmetry axis and I is the moment of inertia. Proton exchange for pseudo-octahedral (or pseudos-quare-pyramidal) M−H_2 complexes, as exemplified in Figure 1 and other previously studied H_2 complexes, is described by the motion of a rigid rotor on an APES dominated by a harmonic 2-fold potential (n = 2; Figure 1) set up, for example, by π-backbonding interactions with the M−P in-plane bonds, whereas methyl group rotation is treated with a 3-fold APES (n = 3; Figure 3, left).[48]

To solve eq 4 we adopt the approach[49] of starting with the free 1-D rotor, V_n = 0, and take as basis the spatial eigenstates of L_z having rotor energies, E_m, eq 5,

$$|m\rangle = \frac{1}{\sqrt{2\pi}}e^{im\phi} \quad m = 0, \pm1, \pm2, \ldots$$
$$E_m = m^2\frac{h^2}{2I} \equiv m^2B \tag{5}$$

where B = 60.8 cm^{-1} for unperturbed $^1H_2$ is reduced to ∼40−50 cm^{-1} because the H_2 is stretched by covalency with M.[3,15] We then solve the matrix eigenvalue problem generated by introducing $V_n(\varphi)$, which has matrix elements:

$$\langle m|V_n(\phi)|m'\rangle = \frac{V_n}{2}\delta_{m,m'} - \frac{V_n}{4}\delta_{m,m'\pm n} \tag{6}$$

As V_n increases and free rotation becomes progressively hindered, the rotor states mix and shift in energy, eventually reaching the limit in which H_2 tunnels (or "hops") among states localized in the APES wells. In all cases of interest, H_2 rotation/exchange involves tunneling through barriers that are far higher in energy than the separation between low-lying states ($V_n \gg B$).

The spatial energies for H_2 rotation relative to the ground-state energy (ΔE) on a 2-fold APES with n = 2 potential (Figure 1) are plotted as a function of barrier height in Figure 7A; the energies are given as the ratio to the rotational constant, $\Delta E/B$. To calibrate these computations, for pseudo-octahedral complexes a barrier height of ∼700 cm^{-1} (V_n/B ∼ 15−18) is common, leading to a tunnel splitting between ground and first-excited state, Δ/B ∼ 0.03.[1]

At first glance, it might seem that the dynamics of exchange for Co−H_2 within the idealized trigonal symmetry of the MP_3 plane should be treated like that of a CH_3/NH_3 group, with a 3-fold APES for H_2 rotation describable by a harmonic potential, n = 3 (Figure 2, left, and Figure S1, Supporting Information).[48] This problem can correspondingly be treated as the result of mixing of free 1-D rotor states by the n = 3 trigonal potential.[49] However, the protons of the trigonal M−H_2 are *not* exchanged by a rotation of $2\pi/3$, and are *only* exchanged by an energetically degenerate π rotation, regardless of additional elements of molecular symmetry, such as a 3-fold barrier. As a result, the treatment of H_2 rotation/exchange in complexes such as those of Figure 2 must be described as the direct product of the C_2 symmetry of exchange with the C_3 rotational symmetry of the molecular scaffold. Thus, H_2 rotation within trigonally symmetric Co−H_2 and Fe−H_2 in fact would occur on an APES of C_6 symmetry, created by a barrier to rotation with a *6-fold* potential n = 6 (Figure 2, right). More generally, in a complex with molecular C_n symmetry, when is n even, H_2 rotation occurs on an APES having the molecular symmetry, but when n is odd, H_2 rotation necessarily occurs on an APES of symmetry C_{2n}. This "doubling" in the order of the barrier potential is highly significant because the higher the order of rotational symmetry, the less influence a rotational barrier of a given height has on H_2 rotation. The calculations presented in Figure 7 reveal the differences between H_2 rotation in a 6-fold versus a 2-fold potential.

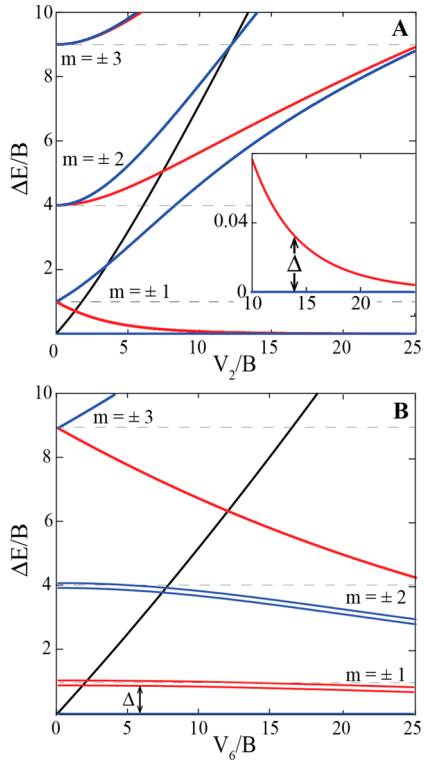

Figure 7. Energies for states of the M−H_2 rotor relative to the ground state energy (ΔE) as a function of barrier height; all energies are plotted in units of the rotational constant ($\Delta E/B$, V_n/B). (A) 2-fold (n = 2) rotational potential (eq 4), plotted as a function of V_2. (B) Energy level differences for 6-fold (n = 6) rotational potential, plotted as a function of V_6/B. As noted in text, at high V_6/B the six lowest levels shown become a representation of the C_6 group; doublets degenerate by symmetry (E) are denoted by double lines. States symmetric to 2-fold rotation, blue; antisymmetric, red; relative barrier heights, black.

For a free rotor (V_i = 0), the nondegenerate ground state is uniformly delocalized around the rotation axis with zero angular momentum (m = 0); the doubly degenerate excited states at energies $\Delta E/B = m^2$ also are uniformly distributed, but with ± m units of angular momentum. As a V_2 2-fold rotational barrier is progressively introduced, more and more states fall below the top of the barrier (Figure 7A) and the energy manifold becomes localized doublets that are symmetric/

dx.doi.org/10.1021/ja508117h | J. Am. Chem. Soc. 2014, 136, 14998−15009

antisymmetric (S/AS) with respect to exchange (e.g., ref[4]). In particular, the angular momentum of the degenerate $m = \pm 1$ states is quenched immediately (Figure S2, Supporting Information) and the two levels split into real even (S) and odd (AS) functions (Figure 7A). The gap between the AS first-excited state and the S ground state, Δ, decreases with increasing V_2, and both of these states localize within the potential wells at $\varphi = 0°$ and 180°, with negligible values for the wave function within the barrier by $V_2/B < 5$. As shown in Figure 7A, the excitation energy, Δ, between the ground pair of S, AS orbitals is decreased to values observed by INS and by NMR for $V_2/B < 15-20$.

In contrast, for the V_6 6-fold potential created by the 3-fold molecular symmetry in conjunction with invariance of H_2 to rotation by π, the energies of the free-rotor states are minimally perturbed even by very high barriers, Figure 7B. Thus, by $V_6/B = 20$, the energy of the $m_s = \pm 1$ states, which remain degenerate, only drops relative to the $m_s = 0$ level from $\Delta/B = 1$ to $\Delta/B \sim 0.85$. Moreover, the ground rotational state is perturbed, but the probability density remains high within the barriers, only decreasing to ~50% of its unperturbed value, with a corresponding increase within the potential "wells." Correspondingly, the angular momentum of the $|m| = 1$ states is decreased only by about 5% for $V_6/B = 20$, and by only 13% even for $V_6/B = 40$ (Figure S2, Supporting Information). As V_6/B increases the energy manifold becomes sextets that comprise the irreducible representations of C_6 (two doublets and two singlets).

This difference between the response to the two potentials is easily understood calculationally and physically. Considering the mixing of free rotor states by V_n, eq 6. Whereas V_2 couples the degenerate $m = \pm 1$ levels to each other, and thus they split linearly as V_2 is applied, the nearest levels that are coupled to $m = \pm 1$ by V_6 are $m = \pm 5$, at an unperturbed energy higher by 24B. Viewed physically, the 'impedance' to rotation offered by a potential increases linearly with the number of its barriers, but the effectiveness of each barrier decreases exponentially with a decrease in width. A six-fold potential has three times the number of barriers to rotation as a two-fold potential, but each barrier is three times smaller in width. As a result, one may crudely view V_6 as being $3\exp(-3) \sim 0.15$ as effective in impeding rotation as V_2 for equal heights. Indeed, the "high-barrier" regime, in which the H_2 is excluded from the barrier regions and tunnels among the six APES wells, is only approached with unphysically high barriers, $V_6/B > 100$. In short, a truly trigonal M−H_2 complex necessarily *should* exhibit rotor-like behavior that is only very weakly perturbed by its molecular environment, and thus H_2 exchange *should* be subject to the quantum statistical control of the H_2 spin state in the spatially symmetric ground rotational state. This argument is obviously generalizable: for C_n rotational symmetry, the influence of the barrier strongly decreases with increasing n.

PJT Control of H_2 Rotation in Co−H_2 and Fe−H_2. In the paradigmatic case of the pseudo-octahedral complex in Figure 1, a 2-fold barrier to H_2 rotation arises because the coordinated CO ligands are stronger π acceptors than the coordinated phosphines. As a result, the W(5d) → $H_2(\sigma^*)$ backbonding interaction is stronger when the H_2 ligand is oriented along the P−W−P vector rather than along the C−W−C vector. In contrast, M → H_2 π-backbonding cannot generate a rotational barrier for a trigonally symmetric H_2 complex. In trigonal symmetry, the electron density of the filled $(d\pi)^4$ orbitally degenerate doublet that participates in backbonding, $(e)^4 = [|m_L \pm 1\rangle]^4$ (Figure 3), is cylindrically symmetrical and thus backbonding can stabilize the M−H_2 bond, but cannot generate a rotational barrier.

Of course, as discussed above, the JT effect converts the electronic degeneracy of the Co−H_2 and Fe−H_2 complexes of Figure 1 into a vibronic degeneracy in which the complex is dynamically distorted. However, we propose that a dynamic linear JT would maintain free (barrierless) 1-D rotation about the M−H_2 axis, with the pseudorotating "in-plane" distortion coupling to the H_2 orientation via the backbonding interaction, and with the distortion of the MP_3 "triangle" thus following the H_2 ligand as implied by the Born−Oppenheimer approximation.[50] In this case, only noncovalent interactions of H_2 with the molecular framework would introduce a fixed spatial barrier to H_2 rotations, a dominantly 3-fold barrier that would be converted to a V_6 APES for H_2 exchange. We propose that the absence of a backbonding contribution to the V_6 barrier for H_2 rotation in a complex that exhibits idealized trigonal symmetry or a dynamic linear PJT distortion from trigonal, added to the insensitivity of H_2 rotation to *any* V_6 barrier, explains why Co−H_2 exhibits rotor-like behavior, with tunnel splitting (Δ) so large that at 2 K one observes ^{2}H ENDOR but not ^{1}H ENDOR ($\Delta \gtrsim 7$ cm^{-1}).

But, then why does Fe−H_2 behave so differently, exhibiting 2 K ^{1}H ENDOR signals from Fe−H_2, rather than a Pauli-principle suppression of ^{1}H ENDOR? We interpret the difference between the two complexes as arising from differential augmentation of the 6-fold barrier of the idealized trigonal complex by a 2-fold harmonic rotational barrier ($V_2(\varphi)$) that is introduced through the agency of a static quadratic PJT distortion acting in consort with M → H_2 π-backbonding:

$$V(\phi) = \frac{V_6}{2}(1 - \cos(6\phi)) + \frac{V_2}{2}(1 - \cos(2(\phi - \phi_0))) \quad (7)$$

where the angle φ_0 describes the offset ("skewing") of the barrier potentials of different symmetry, relative to each other. Figure S3 (Supporting Information) shows how the incorporation of a V_2 barrier rapidly quenches rotor behavior and lowers the tunnel splitting, much like a V_2 barrier by itself, Figure 7A.

A 2-fold barrier contribution is introduced when the MP_3 equilateral triangle becomes distorted through a static quadratic JT distortion to an isosceles triangle. Consider such triangles with apex at the P associated with an M−P bond defined as lying along $\varphi = 0$. When the static distortion opens the P−M−P angle involving the other two phosphines and generates an isosceles triangle with vertex angle greater than 60°, as detailed in the Discussion, backbonding generates a V_2 contribution to $V(\varphi)$ with a skew angle of $\varphi_0 = 0$, which favors an H_2 orientation along the unique M−P bond, as illustrated in the calculated APES of Figure 8, left. When the distortion instead closes the P−M−P angle for the other two phosphines, generating a "compressed" isosceles triangle with vertex angle less than 60° (Figure 8 right), backbonding then generates a V_2 contribution to $V(\varphi)$ with a skew angle of $\varphi_0 = \pi/2$.[51] In this case the resultant APES sum-potential no longer has energy minima for H_2 orientations along the priority M−P bond, $\varphi = 0, \pi$, instead retaining *two* equivalent pairs of energy minima aligned with the other two M−P bonds at $\varphi = \pm 2\pi/3$ (Figure 8 right). Correspondingly, as illustrated in Figure 9, upper, the H_2 rotational wave function along the priority M−P bond is

dx.doi.org/10.1021/ja508117h | J. Am. Chem. Soc. 2014, 136, 14998−15009

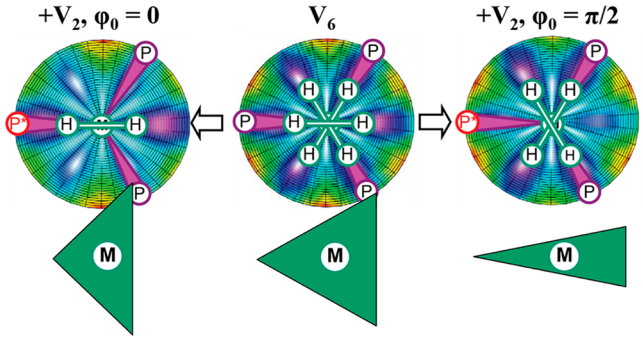

Figure 8. Schematic representation of $V(\varphi)$ for H_2 rotation in a trigonal M−H_2 complex (center) $V(\varphi)$= $V_6(\varphi)$ and with JT distortion along one M−P bond that causes a distortion from equilateral to isosceles triangles with (left) vertex angle >60° and (right) < 60°, thereby respectively introducing a $V_2(\varphi)$ contribution (eq 7) that is characterized respectively by $V_2/V_6 < 0$ (left) or $V_2/V_6 > 0$, $\varphi_0 = 0$ (right).

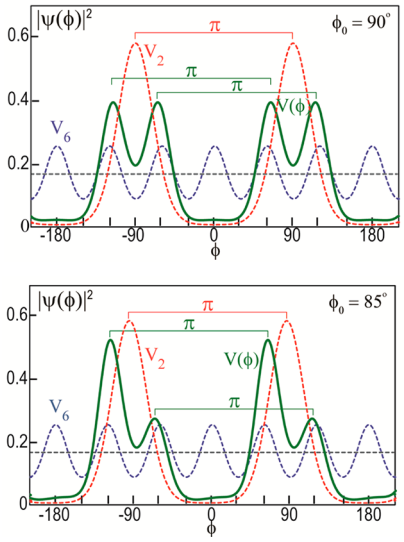

Figure 9. Ground state probability densities for: black, dashed, free rotor; red, 2-fold potential, and blue, 6-fold potential, both with V_n/B = +20; green, sum-potential $V(\varphi)$ (eq 7) with V_6/B = +20, V_2/B = +8. Upper: φ_0 = 90. Lower: φ_0 = 85. Note, as discussed in text, V_2, $V_6 > 0$ is required by the neutron structure.

suppressed, and exhibits two favored H_2 orientations, aligned with the two "nonpriority" M−P bonds at $\varphi = \pm 2\pi/3$. This type of distortion creates an idealized version of the structure found by neutron diffraction, described below. Computations with the sum-potential $V(\varphi)$ (eq 7) show that the large tunnel splitting (relatively weak perturbation of the free-rotor states) implied by the quantum-statistical control of the ^{1,2}H ENDOR of Co−H_2, $\Delta > 7$ cm^{-1}, requires a rather small V_2 barrier height for Co−H_2, $V_2 < 250$ cm^{-1}.

The hyperfine averaging observed for Fe−H_2 led us to suggest that its H_2 rotational dynamics are dominated by tunneling/hopping through a rotation angle of $2\pi/3$ between the two high-occupancy orientations aligned with M−P bonds,[20] precisely as calculated for the PJT distortion described in Figure 8, right. This process does not exchange hydrons and thus would not be subject to exclusion principle constraints, and thus explains why ^{1}H ENDOR signals are observable for Fe−H_2. This process also explain why the ^{1}H dipolar hyperfine interaction was rotated by $\beta = 6°$, away from the $g_\parallel$ axis of the complex, as opposed to the $\beta \sim 15°$ for static Fe−H_2 or $\beta = 0°$ found for the complete rotational averaging of Co−HD/D_2. Direct computations in fact show that an apparent angle $\beta \approx 6°$ would result from averaging by this nonexchanging rotational tunneling of $2\pi/3$. 1-D rotor computations indicate that the strong quenching of the H_2 rotation in Fe−H_2 (strong perturbation of free-rotor states) requires that V_2 must be at least double that for Co−H_2, namely $V_2 > 500$ cm^{-1}.

Neutron-Diffraction Structure of Co−H_2. Neutron diffraction, which relies on the scattering cross section of nuclei, is ideal for determining the atomic distances between light atoms like hydrogen. The structure of Co−H_2 has been determined at 100 K, at which temperature any structural changes upon cooling in general have produced a limiting low-temperature structure that is appropriate for comparison with the ENDOR measurements at still lower temperature.

The high-resolution single crystal neutron diffraction structure of Co−H_2 clearly resolves the presence of a side-on bound H_2 ligand bound to Co and positioned *trans* to boron. Thus, the structure confirms our initial assignment[19] of Co−H_2 as a cobalt-dihydrogen adduct rather than a cobalt-dihydride complex (Figure 10). The H_2 ligand is disordered over two positions, the major component of disorder having a 68.2% site occupancy.[52] The two orientations are associated with Co−P bonds, presumably a reflection of π-backbonding from filled d orbitals of Co to the empty σ^* orbital of H_2,[1−3] although being somewhat skewed with respect to them, by ∼21.2° and ∼8° for the major and minor disordered components, respectively. The H−H bond distances for both H_2 moieties are identical (0.834(6) and 0.83(2) Å) and slightly elongated from the 0.74 Å bond length[2] of free H_2. These distances are similar to those found in other metal-dihydrogen complexes characterized by neutron diffraction (0.82−0.92 Å)[2,6,11] and closely match those for two iron-dihydrogen adducts (0.81−0.82 Å).[14,53]

The structure shows a deviation of the P−Co−P angles away from the 120° of the idealized C_3 symmetry of the Co−P plane (Table 1), as was also observed in the X-ray diffraction structures of Co−H_2 and the closely related complex, Co−N_2: the P1−Co−P3 angle is distinctly less than the other two P−Co−P angles with P2 at the apex of the triangle, "compressing" the MP_3 triangle and giving the M−P2 bond "priority".[19] The distortion can be attributed to a solid-state "locking in" of the quadratic PJT distortion by crystal packing forces, as is illustrated in the electron density isosurface of the solid-state structure of Co−H_2 (Figure 10).[54]

The isosurface shows that the disordered H_2 ligand is located in the blue-colored triangular cavity and is in close contact with three separate methyl hydrogen atoms from three isopropyl groups on the TPB ligand; any possible residual changes in structure upon further cooling to 2 K would only serve to further enhance this localization. The H_2 orientation with higher occupancy may be favored because it has longer H···H interactions between the H_2 ligand and hydrogen atoms of adjacent methyl groups: the closest H···H contacts from the neutron structure are 2.174(6) Å and 2.096(14) Å for the major and minor components of the H_2 ligand, respectively. These close contacts are likely not present in frozen solutions, where packing forces are not in play. Such "crystal-packing" influences on H_2 rotation are long known.[15] INS measurements of Δ for Fe−H_2 and Co−H_2 in the crystalline state would unambiguously clarify such issues.

dx.doi.org/10.1021/ja508117h | J. Am. Chem. Soc. 2014, 136, 14998−15009

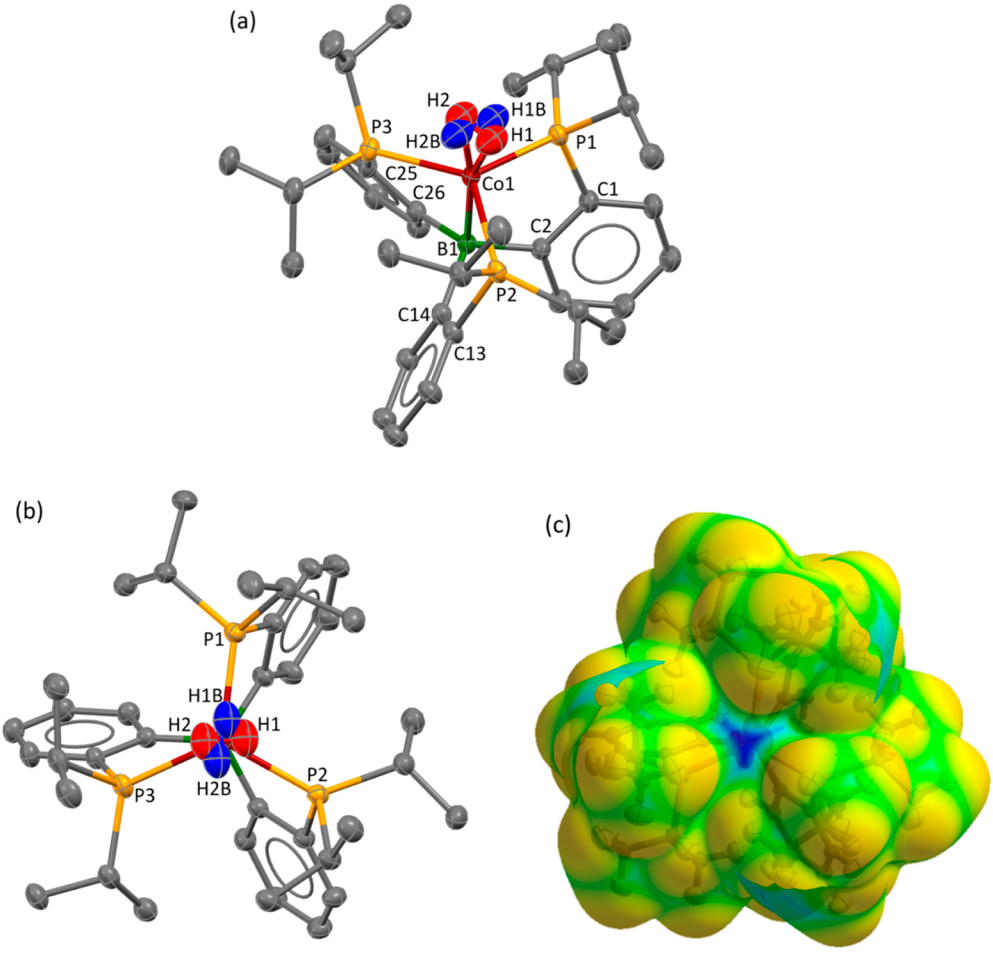

Figure 10. (a) Single crystal neutron diffraction structure of Co−H_2 showing the disordered H_2 ligand in red and blue for the major and minor components, respectively. (b) View down the Co1−B1 vector emphasizing the near parallel orientations of the disordered H_2 ligand with the B1−C26 and P1−Co1 bonds. Ellipsoids are shown at the 50% probability level. Hydrogen atoms on the isopropyl and phenyl groups are omitted for clarity. Purple, Co; green, B; yellow, P; gray, C. (c) A transparent isosurface of the promolecule electron density of Co−H_2 showing the disordered dihydrogen ligand located in the blue colored triangular cavity. The isovalue of 0.0020 e/Å^3 used in the plot is comparable to the expected van der Waals radii.

Table 1. Selected Bond Angles and Distances Determined by X-ray and Neutron Diffraction

Co−H_2	X-ray[a]	neutron
H1−H2 (Å)		0.834 (6)/0.83(2)
M−H1 (Å)		1.659(4)/1.672(7)
M−H2 (Å)		1.664(4)/1.671(7)
M−P1 (Å)	2.2412(3)	2.241(3)
M−P2 (Å)	2.2650(3)	2.280(3)
M−P3 (Å)	2.2750(3)	2.262(3)
M−B (Å)	2.2800(1)	2.287(2)
H1−M−H2 (deg)		29.03(11)/28.91(14)
P1−M−P3 (deg)	119.00(1)	119.40(12)
P1−M−P2 (deg)	110.97(1)	111.92(11)
P2−M−P3 (deg)	124.97(1)	123.93(11)

[a]Ref 19.

Correspondence of Neutron Structure and 1-D Rotor Calculations. This localization of the H_2 ligand in two orientations, each aligned roughly with an M−P bond, is shown above to be expected for a PJT distortion to the compressed isosceles triangle found in the structure (Table 1). In this configuration, π-backbonding generates a V_2 potential for H_2 rotation with a skew angle, $\varphi_0 \sim 90°$, relative to the V_6 potential along the priority bond; when combined with the V_6 potential (eq 7) the result is energy minima aligned with the two "nonpriority" M−P bonds (Figure 8 right). As shown in Figure 9, upper, a plot of the ground-state rotational wave function for this potential exhibits equal occupancy (probability density) for orientations associated with the other two M−P bonds, while suppressing the probability density of the H_2 orientation associated with the priority M−P bond. However, incorporation of only a slight out-of registry of the potentials, by an offset increment of $\delta\varphi_0 \sim 5°$ from the idealized $\varphi_0 = 90°$, in fact introduces a roughly 2-fold difference in the occupancies of the two favored orientations Figure 9, lower, as observed in the structure. To illustrate the correspondence between the neutron structure and the $V(\varphi)$ sum-potential, Figure 11 superimposes the Co−H_2 structure onto a representation of the APES of Figure 8, right, oriented so as to maximize the overlap of the two H_2 orientations with the potential minima of this surface.

Unsurprisingly, the model does not capture subtler details of the crystalline environment, as can be seen by noting that the two orientations of H_2 do not intersect at the midpoints of the H−H bonds, indicating that the H···H interactions between the

dx.doi.org/10.1021/ja508117h | J. Am. Chem. Soc. 2014, 136, 14998−15009

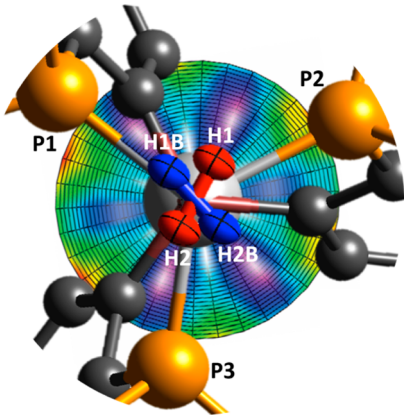

Figure 11. Superposition of the core Co−H_2 neutron diffraction structure on the APES for H_2 rotation of Figure 7, right.

H_2 ligand and the hydrogens of adjacent methyl groups prevents the H_2 from adoption a simple "T-shaped" structure. In principle, such details could also be modeled or investigated by detailed DFT computations, but the inclusion here of the additional complexity would not be compensated by a deepened understanding of the H_2 dynamics.

DISCUSSION

Electronic Structure. Analysis of the *g*-values for Co−H_2 and Fe−H_2 shows that they have the same frontier orbital configurations, a triply occupied, orbitally degenerate ^2E orbital doublet, $(2e)^3 = [x^2 - y^2, xy]^3$, Figure 3. The resulting ^2E state for Co−H_2 and Fe−H_2 is susceptible to the PJT effect,[20] wherein spin−orbit coupling competes with interactions that lower the molecular symmetry. Analysis of the *g*-values for the two complexes shows that the symmetry-lowering matrix element, *V*, which most likely is dominated by the vibronic coupling term (see above) is roughly 2-fold greater for Co−H_2 than for Fe−H_2, a difference that will be discussed below as significantly contributing to differences in the H_2 rotational dynamics of Co−H_2 and Fe−H_2.

The ENDOR measurements provide a sensitive probe of bonding along the L_2−M−E axis, (E = Si for Fe−H_2; E = B for Co−H_2). The negative sign of a_{iso} for both complexes indicates that the spin transfer from metal ion to H_2 is dominated by polarization of the axial L_2−M−X four-electron, three-center σ bonds by the unpaired electron on M, and not by symmetry-forbidden direct delocalization of metal spin in the $[x^2 - y^2, xy]^3$ frontier orbitals through backbonding into the $H_2(\sigma^*)$ orbital. Remarkably, $a_{iso}(^1H)$ for Co−H_2 is nearly 4-fold smaller than for Fe−H_2, corresponding to a nearly 4-fold smaller polarization of the H_2−M−E σ bonds than for Fe−H_2. The smaller polarization implies correspondingly *larger* energy gaps between the three H_2−Co−E σ orbitals, the j_a, j = 1−3 of Figure 3.[55,56] The relatively small value of $a_{iso}(^{11}B)$ and the small ^{11}B quadrupole splitting, taken together, point to a Co → B dative bonding interaction as generating the orbital manifold in Figure 3.

H_2 Rotation/Exchange Dynamics in Co−H_2. $^{1,2}H$ ENDOR measurements for the trigonal Co−H_2/D_2/HD complex at 2 K give ^1H signals from the HD complex, ^2H ENDOR signals from the Co−D_2/HD complexes, but *not* ^1H signals from the Co−H_2 complex. This implies that Hydron exchange introduces a quantum-statistical, Pauli-principle requirement that the overall nuclear wave function be antisymmetric to exchange of identical protons (I = 1/2; Fermions), symmetric for identical deuterons (I = 1; Bosons). The complete absence of a ^1H signal from the Co−H_2 complex at 2 K implies that the gap (Δ) between the ^1H-ENDOR-silent, rotationally symmetric ground state and the ^1H-ENDOR-active, rotationally antisymmetric lowest-lying excited state has a lower bound of $\Delta > 7$ cm^{-1}. If one sets aside Co dihydrogen-hydride complexes in which the presence of a *cis* hydride generates a system in which rotation is strongly coupled to interconversion of dihydrogen and hydride ligands, a situation that results in an anomalously low barrier to rotation and large tunnel splitting ($\Delta \sim 20$ cm^{-1}),[13,14,57,58] the lower limit for Δ of Co−H_2 would make its value one of the largest measured. Temperature-dependent ENDOR measurements and/or INS measurements would yield the actual value of Δ.

Regardless of the precise value of Δ for Co−H_2, these findings can be understood as implying unquenched rotor-like behavior that arises because the complex exhibits an idealized 3-fold symmetry. There are two major consequences of this symmetry for H_2 rotation. One is that the APES for H_2 exchange actually is governed by C_6 symmetry, not merely the idealized molecular C_3 symmetry: the protons of trigonal M−H_2 are *not* exchanged by a rotation of $2\pi/3$, as are those of CH_3, but are exchanged *only* by 2-fold rotation around the M−H_2 axis, so the Co−H_2 rotation in fact occurs on an APES of C_6 symmetry (Figure 2). Direct calculation shows that H_2 rotation is only minimally hindered by even extremely high V_6 barriers, whereas the V_2 barrier found to be dominant in most previous studies strongly quenches rotation and localizes H_2. The second major consequence of idealized C_3 molecular symmetry is that π-backbonding does not generate a rotational barrier, as discussed below.

Influences of the Quadratic JT Vibronic Distortion on H_2 Rotation. To create a rotational barrier, the π-backbonding in Fe−H_2 must be "directional", namely, favor particular orientation(s) of H_2. In a pseudo-octahedral M−H_2 complex, e.g., Figure 1, such directionality arises because the in-plane ligands orient the two orbitals of the $(d\pi)^4 = [xz, yz]^4$ pair along the in-plane bonds to W. As H_2 is itself a π-acid, it more favorably competes for dπ electron density with the slightly π-acidic phosphines than the highly π-acidic carbonyls, and thus aligns with the W−P bond vectors. In a hindered-rotor description, this is equivalent to the presence of the APES for H_2 rotation visualized in Figure 1, with energy minima along the bonds to X = P, barrier maxima along the bonds to Y = CO.

In the idealized C_3 symmetry of Figure 2 the electron density of the filled $(d\pi)^4$ orbital doublet is cylindrically symmetrical, so π-backbonding does not generate a rotational barrier, and we argue above that the linear PJT distortion likewise does not generate a barrier. The directional π-backbonding needed to create a barrier is achieved through a static distortion, attributed to the quadratic JT effect, that "picks out" a priority M−P bond, generating an isosceles triangle of phosphines about M. A distortion that closes the P−M−P angle for two phosphines, Figure 8, right, produces an idealization of the structure found by neutron diffraction (Table 1). Such a distortion orients the $(d\pi)^4$ orbitals so that (say) *xz* is aligned with the priority bond and *yz* orthogonal to it, and thereby enhances electron donation from *xz* to the π-acidic phosphines relative to donation from *yz*. The result is a V_2 potential that is skewed relative to the underlying V_6 potential by $\varphi_0 \sim 90°$, Figure 8, right. The outcome of the interplay between V_2 and V_6 contributions to the sum-potential $V(\varphi)$ (eq 2) is a ground-

dx.doi.org/10.1021/ja508117h | J. Am. Chem. Soc. 2014, 136, 14998−15009

state rotational wave function that exhibits high occupancy (probability density) for the pair of H_2 orientations associated with the two nonpriority M−P bonds, while suppressing the H_2 orientation along the priority M−P (Figure 9).

The neutron structure in fact displays just such a pair of orientations (Figure 10). The structure does show a roughly 2-fold difference in occupancy, whereas for a skew angle of $\varphi_0 = 90°$ the sum-potential predicts equal occupancy for the two H_2 orientations (Figure 9, upper). However, as shown in Figure 9, lower, incorporation of only a slight out-of registry of the V_2 and V_6 potentials, by an offset increment of $\delta\varphi_0 \sim 5°$ from the idealized $\varphi_0 = 90°$, introduces a roughly 2-fold difference in the calculated occupancies of the two favored orientation, comparable to that observed in the structure.

Why are H_2 Rotational Dynamics Different for Fe−H_2 and Co−H_2? The discussion to this point indicates that the two complexes exhibit different H_2 rotational dynamics, with strong perturbation of the free-rotor states of Fe−H_2 and much weaker perturbation for Co−H_2, because the V_2 component to the rotational barrier (eq 7) is much larger for Fe−H_2 than for Co−H_2. As we now show, this difference arises because (i) π-backbonding is stronger for Fe than Co, and (ii) so is the JT distortion that enables backbonding to generate a barrier to rotation.

The π-backbonding capabilities of the [(SiP_3)Fe] and [(TPB)Co] fragments may be compared by considering the spectroscopic and structural properties of the previously reported species (SiP_3)Fe(N_2) (Fe−N_2)[59] and (TPB)Co(N_2) (Co−N_2),[19] which are isoelectronic to Fe−H_2 and Co−H_2, respectively. Substantial differences in both the N−N infrared stretching frequencies (2008 cm^{-1} for Fe−N_2 and 2089 cm^{-1} for Co−H_2)[19,59] and the N−N bond lengths (1.125 Å for Fe−N_2 and 1.062 Å for Co−N_2)[19,60] indicate that the M-N_2 π-backbonding is distinctly greater, and the N−N bond thus more activated, in Fe−N_2 than in Co−N_2. The similar π-acceptor abilities and coordination chemistry of N_2 and H_2[61] mean that these trends extend to Fe−H_2 and Co−H_2.

The distortion that introduces the orientation-dependence of the π-backbonding, which in turn generates the V_2 contribution to the rotation barrier, is attributed to quadratic JT coupling, and this too is stronger for Fe−H_2 than for Co−H_2. The g-shifts, $\delta g_{\|}$, show that the linear JT coupling is nearly 2-fold stronger in the Fe−H_2 complex than Co−H_2, and this in turn implies a greater enhancement of the static quadratic distortion of Fe−H_2. Thus, both of the two factors needed to generate a strong V_2 component to the barrier to H_2 rotation in the JT-active trigonal complexes of Figure 2 are greater for Fe−H_2 than for Co−H_2.

The neutron diffraction structure of Co−H_2 visualizes the distortion to the compressed isosceles triangle of Figure 8, right, and it further suggests that the observed localization involves the effects of crystal packing forces that quench rotation, as illustrated in the electron density isosurface (Figure 10). The possibility of such differential localization in solution vs solid can be addressed with INS measurements.

In summary, the EPR/ENDOR measurements reported here reveal that the Co−H_2 complex in frozen solution at 2 K shows rotor-like behavior with quantum statistical correlation between the exchange symmetry of H_2 spatial and nuclear-spin states, in contrast to Fe−H_2, which exhibits nonexchanging rotational H_2 tunneling/hopping between energy minima separated by $2\pi/3$. H_2 exchange in the idealized trigonal (C_3) symmetry (Figure 2) is shown to occur on a 6-fold (C_6) symmetric APES. However, both complexes exhibit a quadratic JT distortion from the idealized MP_3 equilateral triangle. The analysis of the ENDOR spectra for Fe−H_2 indicated that the distortion may be idealized as the "compressed" (vertex angle less than 60°) isosceles triangle of Figure 8, right, which is shown by quantum 1-D rotor calculations to give rise to enhanced occupancy (probability density) for H_2 orientations associated with the two (nonpriority) M−P bonds, in agreement with the actual occupancies visualized in the neutron diffraction structure of Co−H_2, Figures 10, 11.

The 1-D rotor calculations indicate that such a situation arises because the quadratic JT distortion in combination with 3d → $H_2(\sigma^*)$ π-backbonding introduces a 2-fold rotational barrier. The rotor-like behavior exhibited by Co−H_2 is quenched in Fe−H_2 because stronger π-backbonding in conjunction with a stronger JT distortion in Fe−H_2 creates a larger 2-fold barrier contribution to the barrier for H_2 rotation.

■ ASSOCIATED CONTENT

Ⓢ Supporting Information

Three figures associated with the quantum-mechanics of a 1-D rotor, plus the CIF file for Co−H_2. This material is available free of charge via the Internet at http://pubs.acs.org

■ AUTHOR INFORMATION

Corresponding Authors

jonas.peters@gmail.com
bmh@northwestern.edu

Notes

The authors declare no competing financial interest.

■ ACKNOWLEDGMENTS

This work is dedicated to Prof. Harden M. McConnell, whose recognition of the role of quantum-statistical considerations in paramagnetic resonance spectroscopies occupies but a small place among his numerous scientific contributions, on the occasion of his 87th birthday. We thank Mrs. Junhong (Helen) He, Oak Ridge National Laboratory, for assistance with mounting crystal for neutron diffraction. This work was supported by the National Science Foundation (MCB 1118613, BMH; the NSF Center CHE-1305124, JCP; DGE-0824162, GEC). Research conducted at ORNL's Spallation Neutron Source was sponsored by the Scientific User Facilities Division, Office of Basic Energy Sciences, US Department of Energy, under Contract No. DE-AC05-00OR22725 with UT-Battelle, LLC.

■ REFERENCES

(1) Kubas, G. J. *J. Organomet. Chem.* **2014**, *751*, 33.
(2) Kubas, G. J. *Chem. Rev.* **2007**, *107*, 4152.
(3) Eckert, J. *Spectrochim. Acta* **1992**, *48A*, 363.
(4) Buntkowsky, G.; Limbach, H. H. *J. Low Temp. Phys.* **2006**, *143*, 55.
(5) Farkas, A. *Orthohydrogen, Parahydrogen and Heavy Hydrogen*; Cambridge University Press: London, 1935.
(6) Morris, R. H. *Coord. Chem. Rev.* **2008**, *252*, 2381.
(7) McConnell, H. M. *J. Chem. Phys.* **1958**, *29*, 1422.
(8) Eckert, J.; Kubas, G. J.; Dianoux, A. J. *J. Chem. Phys.* **1988**, *88*, 466.
(9) Eckert, J.; Kubas, G.; Hall, J.; Hay, P. J.; Boyle, C. *J. Am. Chem. Soc.* **1990**, *112*, 2324.
(10) Kubas, G. J., Ed.; *Metal Dihydrogen and σ-Bond Complexes: Structure, Theory and Reactivity*; Kluwer Academic/Plenum Publishers: New York, 2001.

(11) Kubas, G. J.; Burns, C. J.; Eckert, J.; Johnson, S. W.; Larson, A. C.; Vergamini, P. J.; Unkefer, C. J.; Khalsa, G. R. K.; Jackson, S. A.; Eisenstein, O. *J. Am. Chem. Soc.* **1993**, *115*, 569.
(12) Eckert, J.; Blank, H.; Bautista, M. T.; Morris, R. H. *Inorg. Chem.* **1990**, *29*, 747.
(13) Li, S. H.; Hall, M. B.; Eckert, J.; Jensen, C. M.; Albinati, A. *J. Am. Chem. Soc.* **2000**, *122*, 2903.
(14) Vandersluys, L. S.; Eckert, J.; Eisenstein, O.; Hall, J. H.; Huffman, J. C.; Jackson, S. A.; Koetzle, T. F.; Kubas, G. J.; Vergamini, P. J.; Caulton, K. G. *J. Am. Chem. Soc.* **1990**, *112*, 4831.
(15) Eckert, J.; Kubas, G. J. *J. Phys. Chem.* **1993**, *97*, 2378.
(16) Eckert, J.; Albinati, A.; White, R. P.; Bianchini, C.; Peruzzini, M. *Inorg. Chem.* **1992**, *31*, 4241.
(17) Eckert, J.; Albinati, A.; Bucher, U. E.; Venanzi, L. M. *Inorg. Chem.* **1996**, *35*, 1292.
(18) Lowered from 60.8 cm^{-1} by stretching of the H−H bond through M−H_2 covalency.
(19) Suess, D. L. M.; Tsay, C.; Peters, J. C. *J. Am. Chem. Soc.* **2012**, *134*, 14158.
(20) Lee, Y.; Kinney, R. A.; Hoffman, B. M.; Peters, J. C. *J. Am. Chem. Soc.* **2011**, *133*, 16366.
(21) McNaughton, R. L.; Roemelt, M.; Chin, J. M.; Schrock, R. R.; Neese, F.; Hoffman, B. M. *J. Am. Chem. Soc.* **2010**, *132*, 8645.
(22) Bersuker, I. B. *Chem. Rev.* **2013**, *113*, 1351.
(23) Bersuker, I. B. *The Jahn-Teller Effect*, 1st ed.; Cambridge University Press: Cambridge, 2006.
(24) Doslic, N.; Gomzi, V.; Malis, M.; Matanovic, I.; Eckert, J. *Inorg. Chem.* **2011**, *50*, 10740.
(25) Eckert, J.; Webster, C. E.; Hall, M. B.; Albinati, A.; Venanzi, L. M. *Inorg. Chim. Acta* **2002**, *330*, 240.
(26) Hoffman, B. M.; DeRose, V. I.; Ong, J. L.; Davoust, C. E. *J. Magn. Reson.* **1994**, *110*, 52−57.
(27) Epel, B.; Gromov, I.; Stoll, S.; Schweiger, A.; Goldfarb, D. *Concepts Magn. Reson., Part B* **2005**, *26B*, 36.
(28) Jogl, G.; Wang, X.; Mason, S. A.; Kovalevsky, A.; Mustyakimov, M.; Fisher, Z.; Hoffman, C.; Kratky, C.; Langan, P. *Acta Crystallogr., Sect. D: Biol. Crystallogr.* **2011**, *67*, 584.
(29) Zikovsky, J.; Peterson, P. F.; Wang, X. P. P.; Frost, M.; Hoffmann, C. *J. Appl. Crystallogr.* **2011**, *44*, 418.
(30) Schultz, A. J.; Jorgensen, M. R. V.; Wang, X.; Mikkelson, R. L.; Mikkelson, D. J.; Lynch, V. E.; Peterson, P. F.; Green, M. L.; Hoffmann, C. M. *J. Appl. Cryst.* **2014**, *47*, 915.
(31) Schultz, A. J.; Srinivasan, K.; Teller, R. G.; Williams, J. M.; Lukehart, C. M. *J. Am. Chem. Soc.* **1984**, *106*, 999.
(32) Sheldrick, G. M. *Acta Crystallogr., Sect. A: Found. Crystallogr.* **2008**, *A64*, 112.
(33) Farrugia, L. J. *J. Appl. Crystallogr.* **1997**, *30*, 565.
(34) McKinnon, J. J.; Spackman, M. A.; Mitchell, A. S. *Acta Crystallogr., Sect. B: Struct. Sci., Cryst. Eng. Mater.* **2004**, *60*, 627.
(35) Interestingly, simulations of the EPR spectra require an anomalously small ^{59}Co hyperfine coupling, $A(g_{\|}) < 28$ G. This could reflect mixing of the 4p orbital with the orbital doublet, which is allowed in noncentrosymmetric complex such as this one, and is seen in tetrahedral Cu(II) complexes.
(36) Bates, C. A.; Standley, K. J.; Stevens, K. W. H.; Moore, W. S. *Proc. Phys. Soc., London* **1962**, *79*, 73.
(37) Cutsail, G. E., III; Stein, B. W.; Subedi, D.; Smith, J. M.; Kirk, M. L.; Hoffman, B. M. *J. Am. Chem. Soc.* **2014**, *136*, 12323.
(38) The parameter, *k*, can be modulated by 1e−2e mixing associated with "doming" of the M−P_3 core, but this doming is small, and similar, for M = Co and Fe, and the mixing can be ignored.
(39) Weil, J. A.; Bolton, J. R.; Wertz, J. E. *Electron Paramagnetic Resonance: Elementary Theory and Practical Applications*; John Wiley & Sons, Inc: New York, 1994.
(40) For the paradigmatic case in which the absence of a signal solves a problem, see: Doyle, A. C. Silver Blaze. In *Memoirs of Sherlock Holmes*; George Newnes: London, 1894.
(41) Kinney, R. A.; Saouma, C. T.; Peters, J. C.; Hoffman, B. M. *J. Am. Chem. Soc.* **2012**, *134*, 12637.
(42) Snetsinger, P. A.; Chasteen, N. D.; van Willigen, H. *J. Am. Chem. Soc.* **1990**, *112*, 8155.
(43) McConnell, H. M.; Strathdee, J. *Mol. Phys.* **1959**, *2*, 129.
(44) The hyperfine averaging of Co−D_2 also places a lower limit on the rotational frequency, but this is far lower than the lower bound to the "tunnel frequency" inferred above, ($\gtrsim$ 7 K ∼105 MHz.
(45) Doan, P. E. *J. Magn. Reson.* **2011**, *208*, 76.
(46) Unpublished data.
(47) Lucken, E. A. C. *Nuclear Quadrupole Coupling Constants*; Academic Press: New York, 1969.
(48) Prager, M.; Heidemann, A. *Chem. Rev.* **1997**, *97*, 2933.
(49) Flygare, W. H. *Molecular Structure and Dynamics*; Prentice-Hall: Englewood Cliffs, NJ, 1978.
(50) Schatz, G. C.; Ratner, M. A. *Quantum Mechanics in Chemistry*; Prentice Hall: Englewood Cliffs, NJ, 1993.
(51) Figure 8 takes the 6-fold potential as favoring H_2 orientation along the three M−P bonds, $V_6 > 0$; taking $V_6 < 0$ would orient the potential bonds.
(52) The second component of the disordered H_2 was refined to a site occupancy of 25.2%. The remaining 6.8% nuclear density was modeled as a bromide ligand at 2.383(13) Å away from the Co center *trans* to boron, and is attributed to residual Co-Br starting material.
(53) Ricci, J. S.; Koetzle, T. F.; Bautista, M. T.; Hofstede, T. M.; Morris, R. H.; Sawyer, J. F. *J. Am. Chem. Soc.* **1989**, *111*, 8823.
(54) Promolecule is the sum of electron density distribution of spherical atoms within the same molecule: McKinnon, J. J.; Spackman, M. A.; Mitchell, A. S. *Acta Crystallogr., Sect. B: Struct. Sci.* **2004**, *60*, 6270−668.
(55) For perspective, in a perturbation-theory approach, the isotropic coupling would be inversely proportional to the square of the gap between 3a and 2a, with a second term proportional to the gap between 3a and 1a.
(56) McConnell, H. M. *J. Chem. Phys.* **1956**, *24*, 764.
(57) Janak, K. E.; Shin, J. H.; Parkin, G. *J. Am. Chem. Soc.* **2004**, *126*, 13054.
(58) Pons, V.; Conway, S. L.; Green, M. L.; Green, J. C.; Herbert, B. J.; Heinekey, D. M. *Inorg. Chem.* **2004**, *43*, 3475.
(59) Whited, M. T.; Mankad, N. P.; Lee, Y.; Oblad, P. F.; Peters, J. C. *Inorg. Chem.* **2009**, *48*, 2507.
(60) Lee, Y.; Mankad, N. P.; Peters, J. C. *Nat. Chem.* **2010**, *2*, 558.
(61) Morris, R. H.; Earl, K. A.; Luck, R. L.; Lazarowych, N. J.; Sella, A. *Inorg. Chem.* **1987**, *26*, 2674.